NANO LETTERS

Letter

A Systematic Study on the Growth of GaAs Nanowires by Metal#Organic Chemical Vapor Deposition

Cesare Soci, Xin-Yu Bao, David P. R. Aplin, and Deli Wang

Nano Lett., **2008**, 8 (12), 4275-4282 • DOI: 10.1021/nl801986r • Publication Date (Web): 29 October 2008

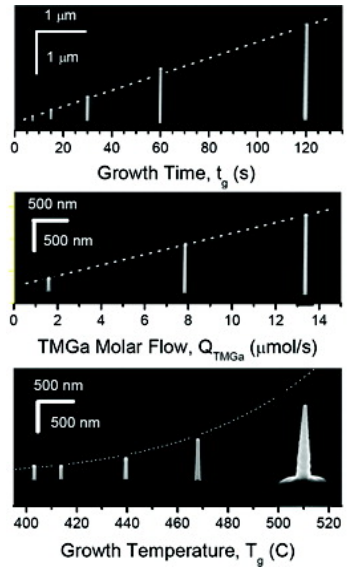

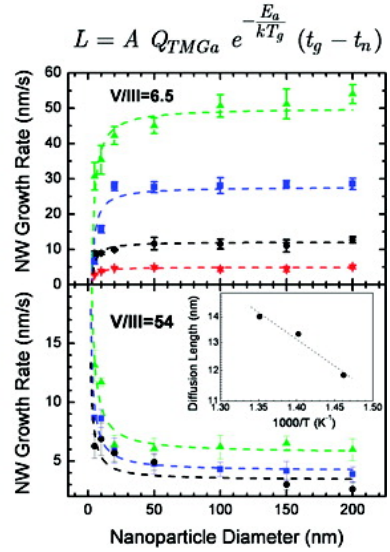

More About This Article

Additional resources and features associated with this article are available within the HTML version:

- Supporting Information
- Access to high resolution figures
- Links to articles and content related to this article
- Copyright permission to reproduce figures and/or text from this article

View the Full Text HTML

NANO LETTERS

2008
Vol. 8, No. 12
4275-4282

A Systematic Study on the Growth of GaAs Nanowires by Metal−Organic Chemical Vapor Deposition

Cesare Soci, Xin-Yu Bao, David P. R. Aplin, and Deli Wang*

Department of Electrical and Computer Engineering, Jacobs School of Engineering, University of California, San Diego, 9500 Gilman Drive, La Jolla, California 92093-0407

Received July 7, 2008; Revised Manuscript Received September 23, 2008

ABSTRACT

The epitaxial growth of GaAs nanowires (NWs) on GaAs(111)B substrates by metal−organic chemical vapor deposition has been systematically investigated as a function of relevant growth parameters, namely, temperature, arsine (AsH_3) and trimethyl-gallium (TMGa) flow rates, growth time, and gold nanoparticle catalyst size. When growing in excess As conditions (V/III molar ratios greater than four), the NW growth rate is independent of AsH_3 concentration, while it is linearly dependent on TMGa concentration, and it is thermally activated. The NW morphology is primarily affected by the growth temperature, with very uniform NWs growing at around 400 °C and severely tapered NWs growing above 500 °C. A simple phenomenological expression that allows prediction of the NW growth rate over a wide range of growth parameters has been derived. The growth rate dependence on the seed nanoparticle size has also been investigated, which reveals valuable information on the role of catalyst supersaturation and Ga surface diffusion in the growth mechanism. The NW growth rate is found to be almost independent of Au nanoparticle size down to diameters of ∼20 nm over a wide range of temperatures and TMGa and AsH_3 molar flows. For smaller NW radii, the growth rate becomes size-dependent and is strongly affected by the V/III molar ratio; at relatively low V/III ratios, smaller NWs grow more slowly due to the Gibbs−Thompson effect, while at higher V/III ratios (V/III > 50), Ga adatom diffusion becomes the dominant mass-transport mechanism, and smaller NWs grow faster than larger ones. The growth-limiting mechanisms in the above growth regimes are finally discussed, and important quantities such as pyrolysis efficiency of the precursors, supersaturation, and surface diffusion length are deduced by comparing the experimental results with the NW growth rates predicted from first principles.

III−V compound semiconductor nanowires are going to play an important role in future advanced technologies such as high-performance field-effect transistors, nanoscale optical sources, photodetectors, chemical/biosensors, and thermoelectric devices.[1−4] In such applications, an unprecedented control over NW morphology, structure, and positioning will be required to allow the reliable manufacturing of practical devices. Among the III−V compound semiconductors, GaAs NWs have attracted much attention due to their possible integration with silicon technology by direct epitaxial growth.[5−7] GaAs NW growth has been achieved by a variety of methods, including growth from solution,[8] molecular beam epitaxy (MBE),[9−13] and metal−organic chemical vapor deposition (MOCVD).[14−17] As commercial MOCVD reactors are becoming common tools for the growth of III−V NWs, the understanding of the NW growth mechanisms and the development of reliable growth protocols that are transferable between different MOCVD systems is becoming an important issue. It was recognized early on that NW growth initiated and promoted by nanoparticle (NP) catalysts proceeds through the vapor−liquid−solid (VLS) mechanism, in which reactants from the vapor phase form a supersaturated liquid alloy inside of the NP, precipitate at the liquid−solid interface, and form the NW crystals.[18] For III−V NW growth by MOCVD, pyrolysis of group III and group V precursors, and incorporation of reactants into the liquid droplet, and eventually into the NW crystal, limit the reaction kinetics; on the other hand, direct impingement and surface diffusion of adatoms in the gas phase to the NP interface and diffusion through the liquid particle toward the liquid−solid interface limit the mass transport. The overall NW growth kinetics is driven by the difference in chemical potential between adatoms in the gas phase and in the solid phase (supersaturation), which is generally reduced during the mass-transport processes. NW growth models by the VLS mechanism can be grouped into two categories,[19,20] the early VLS models, which derive from studies on whisker growth and account for kinetic limitations of NW growth,[21,22] and the more recent diffusion models, which also include mass-transport contributions from the diffusing reactants.[23−25] These models have very distinct predictions for the dependence of the NW growth rate on NP size. The kinetic models

* To whom correspondence should be addressed. E-mail: dwang@ece.ucsd.edu.

10.1021/nl801986r CCC: $40.75
Published on Web 10/29/2008

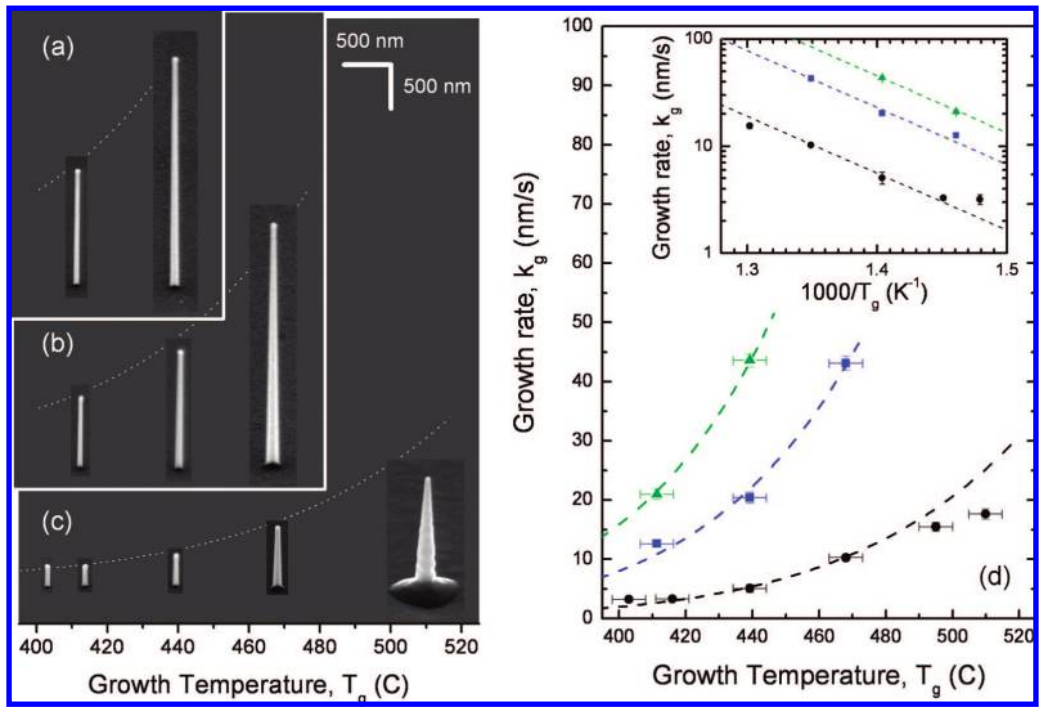

Figure 1. (a−c) SEM micrographs showing the morphology of GaAs NWs as a function of growth temperature (T_g), for various TMGa molar flows of 13.4 (a), 7.8 (b), and 1.6 μmol/s (c). The AsH_3 flow was adjusted to maintain a constant V/III ratio of ~6.5. NW images were recorded on individual growth substrates and recomposed to scale. (d) The corresponding growth rate data: Q_{TMGa} = 13.4 (▲), 7.8 (■), and 1.6 μmol/s (●). The dotted lines are the best fit to the data obtained by eq 1. Inset: Arrhenius plot of the data.

predict that smaller NWs grow more slowly than larger ones due to the decrease in supersaturation in smaller NPs as a result of the larger surface tension (Gibbs−Thompson effect); NW growth cedes below a given critical NW dimension. Conversely, the diffusion models predict that smaller NWs grow faster than larger ones due to the larger sidewall collection area relative to the volume. In contrast to the case of InAs NWs, both of these behaviors have been theoretically predicted and experimentally verified for GaAs[17,19,20,22,25,26] and GaP[24,27] NWs, most likely due to the fact that the diffusion length of Ga adatoms on GaAs surfaces is shorter than that for In adatoms.[28] In this paper, a systematic study on the effects of growth parameters on GaAs NW synthesis by MOCVD is reported, and excellent control of the NW morphology and growth rate has been achieved. The size dependence of the NW growth rate has also been studied in both the kinetically limited and mass-transport-limited regimes; switchover between the two regimes is possible by tuning the V/III molar ratio, which enables the determination of physical quantities such as the pyrolysis efficiency of metal−organic precursors, supersaturation at different stages of VLS growth, and the surface diffusion length of Ga adatoms.

GaAs nanowires were grown using a close-coupled showerhead (CCS) MOCVD system from Thomas Swan Scientific Equipment Ltd., using trimethyl-gallium (TMGa) and arsine (AsH_3) as the gas precursors and hydrogen as the carrier gas. Epitaxial NW growth was achieved on GaAs(111)B substrates, using Au nanoparticles as the seed catalyst. For a typical NW growth, 50 nm diameter Au NPs were dispersed from a water-based colloidal solution (Ted Pella, ~4.5 × 10^{10} NP/mL) on p-type GaAs substrates (used as received without further surface treatment). The NP solution was deposited for ~80 s and dried by N_2 gas, which consistently yielded NP densities of ~5 × 10^6 cm^{-2} (see Supporting Information, Figure S1). For studying the influence of NP size on NW growth, a ~7 × 10^8 NP/mL uniform-density mixture of colloidal solutions (NP diameters of 20, 50, 100, 150, and 200 nm) was prepared, and the deposition time was prolonged to ~85 min to achieve surface densities comparable to the case of monodispersed NP solution. To facilitate NW size differentiation by SEM imaging,[29] NPs with diameters of 5 and 10 nm were deposited onto separate substrates. The chamber pressure during the growth was $P_{chamber}$ = 100 Torr, and the total H_2 gas carrier flow was Q_{H_2} = 20.16 mmol/s. The temperature was raised to the growth temperature in an AsH_3-rich environment,[30] and after a short stabilization time, NW growth was initiated by introducing TMGa to the chamber. Unless otherwise stated, the NW growth time was 60 s.

NW growth via the VLS mechanism is strongly dependent on parameters such as substrate growth temperature (T_g), TMGa molar flow (Q_{TMGa}), AsH_3 molar flow (Q_{AsH_3}), V/III molar ratio (herein defined as V/III = Q_{AsH_3}/Q_{TMGa}), growth time (t_g), and NP catalyst size. Figure 1 shows the temperature dependence of the NW morphology, length (L), and growth rate (k_g) for various TMGa and AsH_3 concentrations. Here, the V/III molar ratio was kept constant (V/III ~ 6.5) by varying Q_{AsH_3} and Q_{TMGa} proportionally from 87.0 to 13.4 μmol/s (Figures 1a and d triangles), 50.2 to 7.8 μmol/s (Figures 1b and d squares), and 10.4 to 1.6 μmol/s (Figures 1c and d circles), respectively. The nanowire growth rate

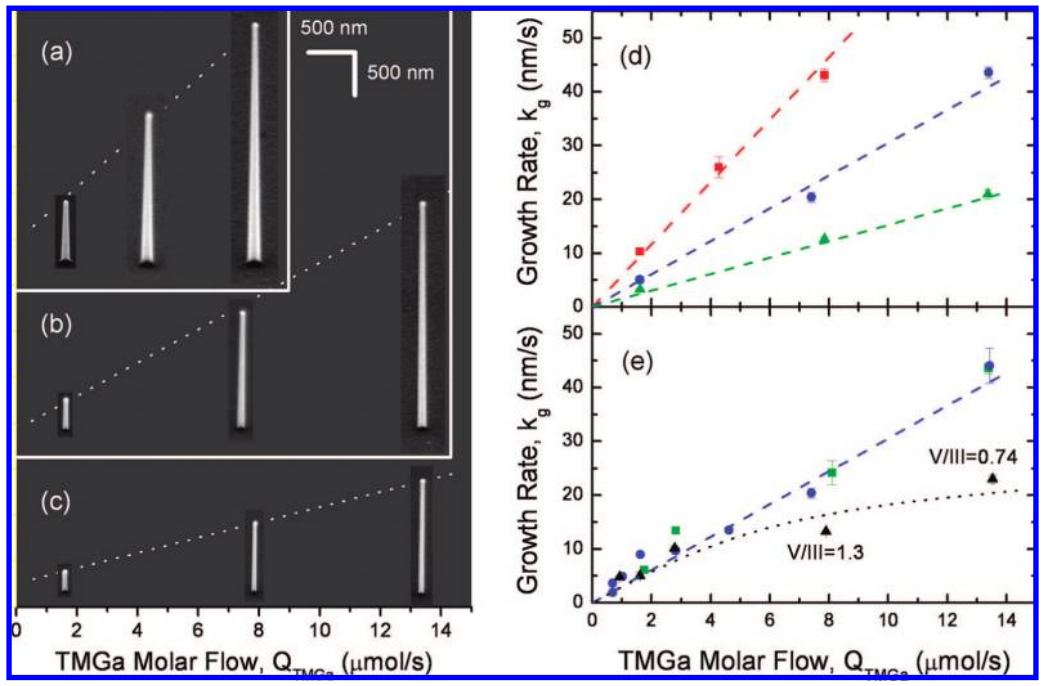

Figure 2. (a−c) SEM micrographs of GaAs NWs as a function of TMGa molar flow for various growth temperatures of 468 (a), 440 (b), and 410 °C (c). In these experiments, the V−III ratio was kept constant at ∼6.5 by adjusting AsH_3 flow. NW images were recorded on individual growth substrates and recomposed to scale. (d) The corresponding growth rate data: T_g = 410 (▲), 440 (●), and 468 °C (■). The dashed lines are the best fit to the data obtained by eq 2. (e) The dependence of NW growth rate on Q_{TMGa} obtained at T_g = 440 °C for various AsH_3 molar flows of 10.4 (▲), 50.2 (●), and 87.0 μmol/s (■); k_g is found to be linearly dependent on Q_{TMGa} and independent of Q_{AsH_3} at high V/III ratios (dashed line), while it depends sublinearly on Q_{TMGa} at low AsH_3 flow (V/III ratios, dotted line).

($k_g = L/t_g$ under the assumption that k_g does not vary with time; see later discussion) shows a thermally activated behavior at the various Q_{TMGa} and Q_{AsH_3} investigated. The dotted lines in Figure 1 represent a simultaneous fit to the three sets of data with the function

$$k_g = K(Q_{TMGa}, Q_{AsH_3})e^{-E_a/kT_g} \quad (1)$$

where the proportionality constant $K(Q_{TMGa}, Q_{AsH_3})$ is a yet unknown function of TMGa and AsH_3 concentration, E_a is the molar activation energy for NW growth, and k is the Boltzmann constant. From the Arrhenius plot displayed in the inset of Figure 1d, the activation energy is $E_a = 24.4 \pm 1.3$ kcal/mol,[31] which is similar to the activation energy of GaAs(111) thin-film growth in the kinetically limited regime (E_a = 22 kcal/mol).[32] The NW morphology is strongly affected by growth temperature (Figures 1a−c), with uniform NWs growing at the lowest temperatures ($T_g \sim 400$ °C) and more tapered NWs growing at the highest temperatures ($T_g > 480$ °C). At high temperatures, the NW growth rate departs from the thermally activated behavior described by eq 1 and reaches saturation (Figure 1d); as previously noted, this is indicative of a radial growth mechanism becoming significant with respect to the VLS mechanism at high temperatures,[14] when the conditions for GaAs thin-film growth are approached. The formation of large islands at the NW bases is also evident in Figure 1c.

Figure 1 shows that the NW growth rate increases by increasing Q_{TMGa} and Q_{AsH_3}. The specific influence of TMGa and AsH_3 molar concentrations is considered in Figure 2, where the data are displayed as a function of Q_{TMGa}. At a constant V/III ratio (Figures 2a−d), the NW length (thus k_g) is linearly dependent on Q_{TMGa} at all growth temperatures investigated of T_g = 468 (Figures 2a and d squares), 440 (Figures 2b and d circles, and 1e), and 410 °C (Figures 1c and d triangles). The NW morphology is almost unaffected by TMGa molar flow, whereas, as noted before, NWs become more tapered at higher growth temperatures (Figures 2a−c). The dashed lines in Figures 2a−c and e and f are linear fits obtained simultaneously on the three sets of data according to

$$k_g = A(Q_{AsH_3})e^{-E_a/kT_g}Q_{TMGa} \quad (2)$$

where, by comparison with eq 1, $K(Q_{TMGa}, Q_{AsH_3}) = A(Q_{AsH_3})\cdot Q_{TMGa}$. In order to determine the dependence of A on Q_{AsH_3} (or equivalently on the V/III ratio), we have conducted the set of experiments shown in Figure 2e at a constant growth temperature (T_g = 440 °C), where the Q_{TMGa} dependence of the growth rate was studied for different AsH_3 molar flows of 10.4 (up triangles), 50.2 (circles), and 87.0 μmol/s (squares). At sufficiently high AsH_3 flow rates (e.g., at high V/III ratios), the NW growth rate follows a linear dependence on Q_{TMGa} similar to the one already observed in Figure 2d for the same growth temperature (dashed line). Further analysis indicates that the NW growth rate is unaffected by arsine concentration when V/III > 4. As shown by the black curve in Figure 2, the growth rate departs from linearity at lower V/III molar ratios when its decrease can be attributed to a lack of As constituents (dotted line);[7,17] nevertheless, NW growth can be achieved at V/III molar ratios as low as 0.74. We can therefore assume that in typical III−V NW growth conditions by MOCVD (i.e., at sufficiently high V/III ratios), the effect of AsH_3 flow on the morphology and the NW growth rate is negligible; from the

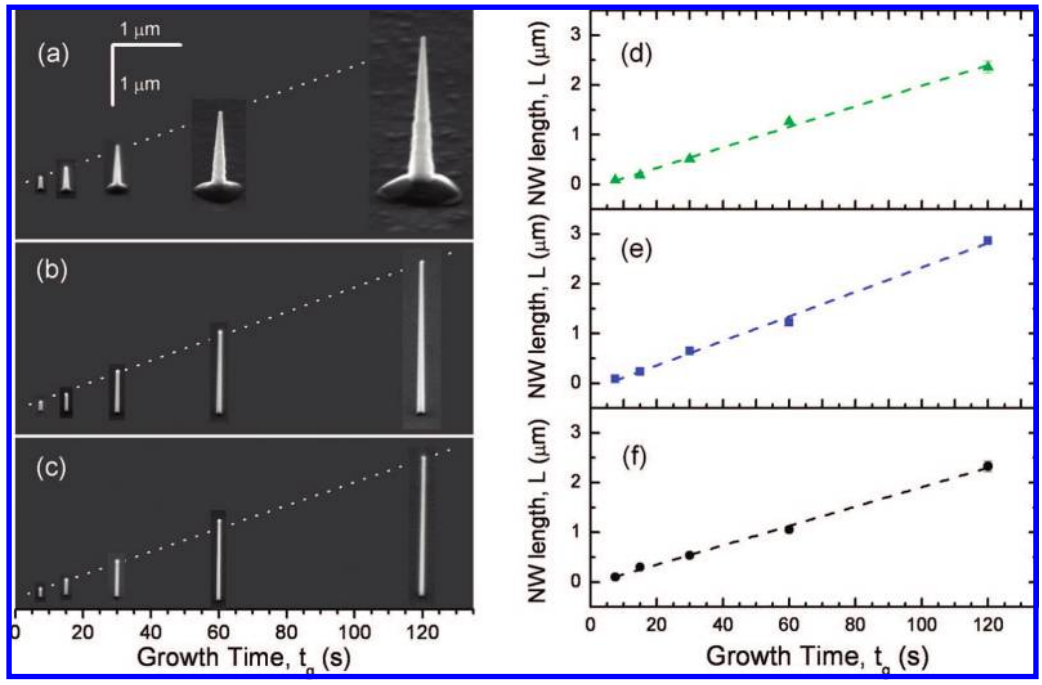

Figure 3. SEM images (a−c) and the corresponding lengths (d−f) of GaAs NWs as a function of growth time (t_g) for various growth temperatures of 510 (a, d), 440 (b, e), and 410 °C (c, f). The TMGa molar flow was 1.6 (a, d), 7.8 (b, e), and 13.4 μmol/s (c, f). AsH_3 flow was varied accordingly to maintain a constant V/III ratio of ~6.5. The dashed lines in (d−f) are the best fit to the data obtained by eq 3. NW images were recorded on individual growth substrates and recomposed to scale.

fittings in Figure 2, we obtain $A(Q_{AsH_3}) = A = 73.6$ nm/mol.

The NW length can be accurately controlled by the growth time. Figure 3 shows the time dependence of the NW length for three different growth temperatures of $T_g = 410$ (Figures 3a,d), 440 (Figures 3b,e), and 510 °C (Figures 3c,f). For the different temperatures investigated, Q_{TMGa} was varied from 13.4 (Figures 3a,d) to 7.8 (Figures 3b,e) and 1.6 μmol/s (Figures 3c,f) in order to obtain comparable NW growth rates. In all cases, the NW length was found to be proportional to growth time, as shown by the linear fit to the data (dashed lines) obtained with

$$L = \Lambda(t_g - t_n) \tag{3}$$

In eq 3, Λ is a proportionality constant, and the nucleation time t_n is introduced to account for a lag between the extrapolation of the linear dependencies in Figure 3 and the time at which TMGa is input to the chamber. From the fittings in Figures 3d−f, we deduce an average nucleation time of $t_n \sim 3.5$ s. The linear dependence of NW length with time implies that the growth rate is independent of growth time, and therefore, the assumption made in eqs 1 and 2 that k_g is independent of time is valid.

Combining eqs 1−3, we can finally derive a phenomenological expression for the NW length involving all of the relevant growth parameters given by

$$L = AQ_{TMGa}e^{-E_a/kT_g}(t_g - t_n) \tag{4}$$

where $A = 7.36$ nm/mol, $E_a = 24.4$ kcal/mol, and $t_n = 3.5$ s. Remarkably, eq 4 allowed reproduction a posteriori of the NW lengths from almost 60 GaAs NW growth runs spanning the entire range of growth parameters allowed in our MOCVD system ($T_g = 403-510$ °C, $Q_{TMGa} = 0.7-13.4$ μmol/s, $Q_{AsH_3} = 10.4-87.0$ μmol/s, and $t_g = 7.5-1600$ s, yielding NW lengths of $L = 0.06-6.38$ μm), on average within 23% of their measured values (see also Supporting Information, Figure S2 and Table S1). A similar approach might be used in future industrial applications requiring highly reproducible NW production with fine control of the morphology.

Since the early experiments on Si nanowhisker growth, the dependence of the growth rate on the seed NP size has proven most useful for understanding the underlying growth mechanism.[33] Reduction of the NW lateral dimensions may also be desirable in future applications targeting large-device integration density or to exploit quantum size effects to engineer the NW electronic properties. Figure 4 shows the dependence of the NW growth rate on Au catalyst NP size. In Figure 4a, NWs were grown at a constant growth temperature of 440 °C and different TMGa molar flows of $Q_{TMGa} = 0.5$ (down triangle), 1.6 (circle), 7.8 (square), and 13.5 μmol/s (up triangle), while in Figure 4b, Q_{TMGa} was 7.8 μmol/s and the growth temperature was varied from 411 (circles) to 440 (squares) and 467 °C (triangles). In all of these cases, the V/III ratio was kept constant at ~6.5 by varying Q_{AsH_3}. As shown in the graphs, there is a mild dependence of the NW growth rate on the NP diameter down to 20 nm, independent of T_g and Q_{TMGa} (see also Supporting Information, Figures S3 and S4). For $d < 20$ nm, the NW growth rate decreases with NP size, which has been commonly attributed to the Gibbs−Thompson effect, and NW growth terminates below a critical radius r_c. Recently, it has been noted that the V/III ratio may significantly affect the NW growth rate dependence on NP size.[17] This was indeed verified in our experiments. Figure 5 shows the NW

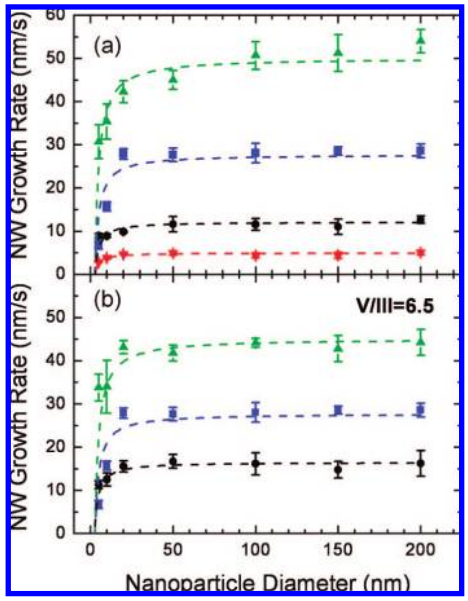

Figure 4. NW growth rate versus Au nanoparticle radius at V/III = 6.5. (a) Constant growth temperature (T_g = 440 °C) and different TMGa molar flow of Q_{TMGa} = 0.5 (▼), 1.6 (●), 7.8 (■), and 13.5 μmol/s (▲); (b) constant TMGa molar flow (Q_{TMGa} = 7.8 μmol/s) and different growth temperatures of T_g = 411 (●), 440 (■), and 467 °C (▲). The dashed lines are a fit to the data according to eq 5, with d_c = 27.5 nm.

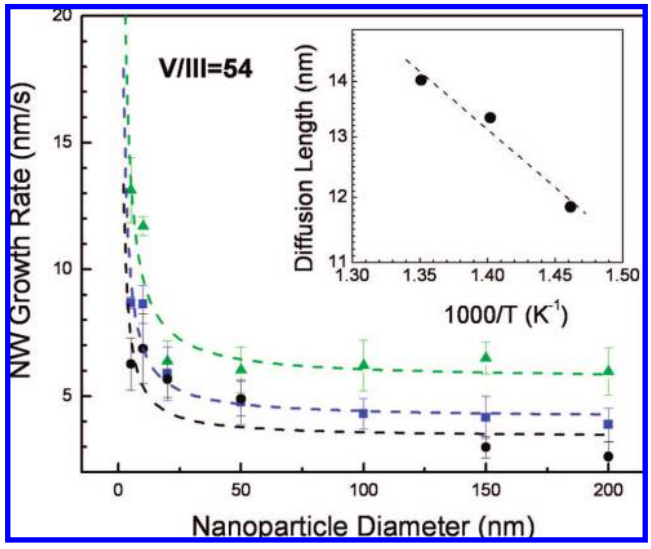

Figure 5. NW growth rate versus Au nanoparticle radius at V/III = 54. The TMGa molar flow was Q_{TMGa} = 0.5 μmol/s, and the growth temperature was T_g = 411 (●), 440 (■), and 467 °C (▲). The solid lines are the best fit to the data according to eq 5. The inset shows the Arrhenius plot of the extracted diffusion length as a function of temperature.

growth rate dependence on NP size obtained at a much higher V/III ratio of ~54 for growth temperatures of 411, 440, and 467 °C. It is remarkable that in these conditions, NWs grown from smaller particles grow faster than NWs grown from larger particles, as expected for diffusion-controlled mass transport of the reactants.

The NW length (growth rate) as expressed in eq 4 can be related to the growth-limiting steps during the MOCVD process. Particularly, it is useful to compare the NW growth rates obtained experimentally with those expected from first principles. For this purpose, we are going to consider the two major mechanisms of supply of the constituent, namely, direct impingement of the reactants onto the metal NP (approximated by a hemisphere of radius r) and contribution from surface diffusion onto the NW sidewalls. On the basis of the results in Figure 2, showing that at typical V/III ratios the NW growth rate is linearly dependent on Q_{TMGa} and almost independent of Q_{AsH_3}, we will assume that the supply of Ga to the growth interface is the major limiting factor. The effect of NP size on supersaturation is also accounted for by the Gibbs−Thompson effect. Under these assumptions, the incident molecular flux of TMGa for a given partial pressure is given by the Hertz−Knudsen equation, and the NW growth rate, $k_g = dL/dt$, can be written as[23,34,35]

$$k_g = \frac{2a^3}{n} \frac{P_\infty (e^{R/r_c} - e^{R/r})}{\sqrt{2\pi m k T_g}} \left(1 + \frac{\lambda}{r}\right) \tag{5}$$

where a is the GaAs lattice constant, n is the number of group V atoms per unit cell, P_∞ is the Ga vapor pressure in equilibrium with a flat surface,[36] m is the mass of the reactant species (Ga atoms), λ is the Ga diffusion length on the NW sidewall surfaces, and r is the NP radius. The Ga sticking coefficient on the Au NP surface is assumed to be unity at the NW growth temperatures. The arguments of the exponential factors in eq 5 depend on the characteristic length R and the critical radius r_c given by

$$R = 2\sigma\Omega/kT \qquad r_c = 2\sigma\Omega/\Delta\mu \tag{6}$$

where σ is the surface energy density at the vapor−liquid interface and Ω is the molar volume of the reactant species in the NP. The $\Delta\mu$ in eq 6 is the chemical potential gradient between the vapor and the liquid phases, where Ga is incorporated into the NP; $\Delta\mu$ is given by[35]

$$\Delta\mu = kT \ln(P_{Ga}/P_\infty) \tag{7}$$

where P_{Ga} is the effective Ga pressure responsible for supersaturation. From eqs 6 and 7, therefore, the supersaturation is given by $\Delta\mu/kT = R/r_c = \ln(P_{Ga}/P_\infty)$. It is known that, despite the large supersaturation values typical of MOCVD reactions, supersaturation is quickly consumed along the reaction coordinates, and epitaxial growth proceeds at nearly equilibrium conditions near the growth interface.[37] P_{Ga} depends on pyrolysis of the TMGa precursor as well as mass transport through the boundary layer at the vapor−liquid interface.[37] Therefore, P_{Ga} is expected to be lower than the Ga partial pressure and can be generally expressed as

$$P_{Ga} = \varepsilon\varepsilon_{pyro} P_{TMGa} \tag{8}$$

where P_{TMGa} indicates the partial pressure of the TMGa precursor in the vapor phase ($P_{TMGa} = \chi_{TMGa} P_{chamber}$, where $\chi_{TMGa} = Q_{TMGa}/(Q_{TMGa} + Q_{AsH_3} + Q_{H_2}) \sim Q_{TMGa}/Q_{H_2}$ is the molar fraction of TMGa and $P_{chamber}$ is the chamber pressure during growth), ε_{pyro} is the temperature-dependent pyrolysis efficiency of TMGa, and ε is an efficiency coefficient that accounts for the reduction in supersaturation at the vapor−liquid interface. As all of the parameters are known from first principles except for ε and ε_{pyro}, eqs 5−8 allow the direct comparison of the growth rate values obtained experimentally with their expected values. For large enough NPs, both the Gibbs−Thompson effect and the contribution from diffusion

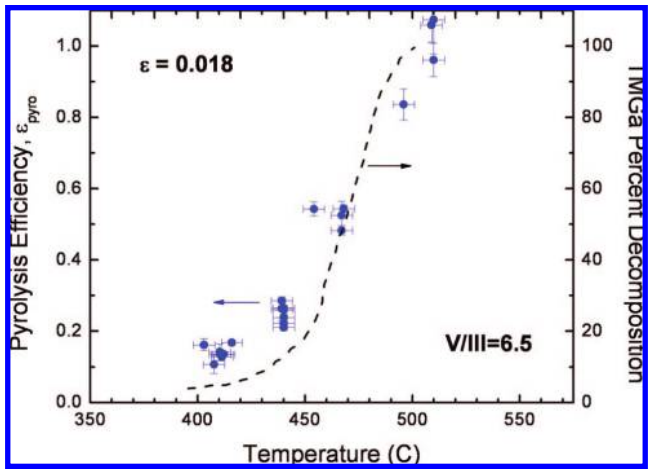

Figure 6. Growth efficiency derived from the data in Figures 1−3 and eq 6 (●). The dashed curve represents the decomposition efficiency for TMGa in the presence of a GaAs(111) suface from ref 38.

can be neglected, and eq 5 reduces to $k_g \sim (2a^3/n)(P_{Ga}/(2\pi kT)^{1/2})$; compare to eq 4, from which the product $\varepsilon \cdot \varepsilon_{pyro}$ can then be derived. Figure 6 shows the TMGa pyrolysis efficiency extracted from our data (circles) with input parameters of $P_{chamber} = 13.33$ kPa, $a = 0.565$ nm, $n = 4$, and $m \sim 1.158 \times 10^{-25}$ kg and assuming complete TMGa pyrolysis at ~510 °C, that is, $\varepsilon = 0.018$; the decomposition efficiency for pure TMGa in the presence of a GaAs(111) surface from ref 38 is also displayed for comparison (dashed line). The good match between the extracted efficiency and the one found in the literature suggests that pyrolysis of the TMGa precursor is the predominant kinetic limitation to the NW growth. Furthermore, the fact that the pyrolysis efficiency obtained for NW growth is comparable to the one for pure TMGa indicates a negligible catalytic effect of Au NPs on the pyrolysis,[34] consistent with the similarity between the activation energy derived in Figure 1 and that of GaAs thin-film growth. We also notice that a similar value of ε could be obtained in ref 24, indicating that the effective pressure of Ga species that are incorporated into the NP is lower than the percentage of TMGa that decomposes. This could be due to higher-order reactions yielding Ga from TMGa[39] (which is not accounted for by the TMGa decomposition efficiency) or, as previously noted, to the reduction in supersaturation.

The dependence of NW growth rate on NP size is profound and interrelated to the growth conditions, such as the V/III molar ratio. At a low V/III ratio (V/III ~ 6.5), NWs grown from smaller size NPs grow slower than those from larger size NPs, as predicted by the Gibbs−Thompson effect (Figure 4). From the fittings in Figure 4 (eq 5, neglecting the contribution from diffusion), we extracted a critical diameter of $d_c = 2r_c = 2.75$ nm, below which NW growth ceases.[40] Considering the NP to be pure gold (i.e., neglecting the relatively small amount of Ga alloyed in the NP), we have $\sigma = 1.237$ J/m^2 and $\Omega = 10.20$ cm^3/mol, which, according to eq 6, yields $\Delta\mu \sim 4$ kcal/mol and a supersaturation of $\Delta\mu/kT \sim 3$. These values are typical for liquid-phase epitaxy growth conditions[41] and must be related to crystallization at the liquid−solid interface. The $\Delta\mu$ derived from the analysis of the Gibbs−Thompson effect is lower than the one predicted by eqs 7 and 8, with $\varepsilon = 0.018$ and ε_{pyro} given in Figure 6 ($\Delta\mu \sim 25$ kcal/mol); this further reduction in supersaturation could be due to mass transport through the liquid NP toward the liquid−solid interface or to the crystallization process during the VLS NW growth. At higher V/III ratios (V/III ~ 54), NWs from smaller size NPs grow faster than those from larger size NPs, and the size dependence of the growth rate follows the trend expected for diffusion-limited growth (Figure 5). Since an increase in supersaturation is unlikely to happen in As-rich conditions, this indicates a relative increase in the contribution from surface diffusion. In ref 17, the mechanism responsible for the switchover between the thermodynamically limited to diffusion-limited growth regime has already been attributed to the increase of the NW growth rate at high As flows, which determines a depletion of Ga constituents available for crystallization. Another possibility is the increase in the Ga surface diffusion length at high V/III ratios due to GaAs surface reconstruction[42] or some sort of surface passivation mechanism due to the abundance of As atoms; similar effects may be competing with the decrease of λ in As-rich conditions, which is usually observed due to faster Ga incorporation rate.[43] The fittings in Figure 5 according to eq 5 (where the Gibbs−Thompson effect has now been neglected) yielded Ga diffusion length values on the order of $\lambda \sim 10$ nm.[44] Such a short surface diffusion length is consistent with the linear dependence of the NW length on growth time (Figure 3), with the absence of surface island formation at the optimal NW growth conditions (low growth temperatures) and with the small NW tapering.[31] The diffusion length (here intended as the average adatom migration distance before incorporation)[44] is given by $\lambda = (D\tau_d)^{1/2} = \alpha \exp(-\Delta E_{diff}/2kT)$, where D is the diffusivity, $1/\tau_d$ is the adatom incorporation rate, α is a coefficient that may depend on growth conditions (such as surface reconstruction, V/III ratio, etc.), and ΔE_{diff} is the activation energy for adatom migration; therefore, λ is expected to show a thermally activated behavior. The inset of Figure 5 shows the Arrhenius plot of the extracted diffusion length as a function of temperature, from which an activation energy of $\Delta E_{diff} \sim 0.3$ eV (6.9 kcal/mol) is deduced. At high growth temperatures, the increase of Ga diffusion length is also responsible for the formation of the large NW bases observed in Figure 1.

In summary, the morphology of GaAs NWs grown epitaxially on GaAs(111)B substrates can be accurately controlled by adjusting the growth temperature, and the NW growth rate is well predicted by eq 4 in a wide range of AsH_3 and TMGa molar flows and growth temperatures. The pyrolysis efficiency of TMGa seems to be the major factor limiting the growth kinetics at the optimal GaAs NW growth temperatures, similar to the case of GaAs film growth by MOCVD. As observed by the NP size dependence of the growth rate, a transition from kinetically limited to mass-transport-limited growth can be induced at high V/III molar ratios, which allows determination of important growth parameters such as supersaturation and Ga adatom surface diffusion lengths. Supersaturation is consumed as the VLS

reaction proceeds and is lowered by pyrolysis of the precursors, mass transport, and surface reactions to values comparable to liquid-phase epitaxy conditions. The Ga surface diffusion length appears to be very short, on the order of 10 nm, which is consistent with the linear dependence of the NW length on growth time, the absence of island formation at low growth temperatures, and the small NW tapering. The short Ga surface diffusion length allows observation of the Gibbs−Thompson effect for NP diameters smaller than ~20 nm, and at low V/III ratios, NW growth ceases for diameters smaller than $d_c \sim 3$ nm.

Acknowledgment. We are grateful to Shady A. Dayeh for the useful discussions regarding the NW growth mechanism. We would like to thank the Office of Naval Research (ONR-nanoelectronics), the National Science Foundation (ECS-0506902), and Sharp Laboratories of America for financial support.

Supporting Information Available: Large-area SEM image of a typical GaAs NW growth (Figure S1), comparison between the measured and predicted NW length for a wide range of growth parameters (Figure S2 and Table S1), and SEM images showing the size dependence of the NW length on seed NP size (Figures S3 and S4). This material is available free of charge via the Internet at http://pubs.acs.org.

References

(1) Thelander, C.; Agarwal, P.; Brongersma, S.; Eymery, J.; Feiner, L. F.; Forchel, A.; Scheffler, M.; Riess, W.; Ohlsson, B. J.; Gosele, U.; Samuelson, L. Nanowire-based one-dimensional electronics. *Mater. Today* **2006**, *9* (10), 28–35.

(2) Li, Y.; Qian, F.; Xiang, J.; Lieber, C. M. Nanowire electronic and optoelectronic devices. *Mater. Today* **2006**, *9* (10), 18–27.

(3) Pauzauskie, P. J.; Yang, P. Nanowire photonics. *Mater. Today* **2006**, *9* (10), 36–45.

(4) Heremans, J. Nanometer-scale thermoelectric materials. *Springer Handb. Nanotechnol.* **2007**, *345* (373), 345.

(5) Bakkers, E. P. A. M.; Borgstrom, M. T.; Verheijen, M. A. Epitaxial growth of III-V nanowires on group IV substrates. *MRS Bull.* **2007**, *32* (2), 117–122.

(6) Martensson, T.; Svensson, C. P. T.; Wacaser, B. A.; Larsson, M. W.; Seifert, W.; Deppert, K.; Gustafsson, A.; Wallenberg, L. R.; Samuelson, L. Epitaxial III-V nanowires on silicon. *Nano Lett.* **2004**, *4* (10), 1987–1990.

(7) Bao, X.-Y.; Soci, C.; Susac, D.; Bratvold, J.; Aplin, D. P. R.; Wei, W.; Chen, C.-Y.; Dayeh, S. A. D.; Kavanagh, K. L.; Wang, D. Heteroepitaxial growth of vertical GaAs nanowires on Si (111) substrates by Metal-Organic Chemical Vapor Deposition. *Nano Lett.* **2008**, in press.

(8) Yu, H.; Buhro, W. E. Solution-liquid-solid growth of soluble GaAs nanowires. *Adv. Mater.* **2003**, *15* (5), 416.

(9) Plante, M. C.; LaPierre, R. R. Au-assisted growth of GaAs nanowires by gas source molecular beam epitaxy: Tapering, sidewall faceting and crystal structure. *J. Cryst. Growth* **2008**, *310* (2), 356–363.

(10) Wu, Z. H.; Mei, X. Y.; Kim, D.; Blumin, M.; Ruda, H. E. Growth of Au-catalyzed ordered GaAs nanowire arrays by molecular-beam epitaxy. *Appl. Phys. Lett.* **2002**, *81* (27), 5177–5179.

(11) Harmand, J. C.; Tchernycheva, M.; Patriarche, G.; Travers, L.; Glas, F.; Cirlin, G. GaAs nanowires formed by Au-assisted molecular beam epitaxy: Effect of growth temperature. *J. Cryst. Growth* **2007**, *301*, 853–856.

(12) Harmand, J. C.; Patriarche, G.; Pere-Laperne, N.; Merat-Combes, M. N.; Travers, L.; Glas, F. Analysis of vapor-liquid-solid mechanism in Au-assisted GaAs nanowire growth. *Appl. Phys. Lett.* **2005**, *87* (20), 203101.

(13) Piccin, M.; Bais, G.; Grillo, V.; Jabeen, F.; De Franceschi, S.; Carlino, E.; Lazzarino, M.; Romanato, F.; Businaro, L.; Rubini, S.; Martelli, F.; Franciosi, A. Growth by molecular beam epitaxy and electrical characterization of GaAs nanowires. *Physica E* **2007**, *37* (1−2), 134–137.

(14) Borgstrom, M.; Deppert, K.; Samuelson, L.; Seifert, W. Size- and shape-controlled GaAs nano-whiskers grown by MOVPE: a growth study. *J. Cryst. Growth* **2004**, *260* (1−2), 18–22.

(15) Paiano, P.; Prete, P.; Speiser, E.; Lovergine, N.; Richter, W.; Tapfer, L.; Mancini, A. M. GaAs nanowires grown by Au-catalyst-assisted MOVPE using tertiarybutylarsine as group-V precursor. *J. Cryst. Growth* **2007**, *298*, 620–624.

(16) Joyce, H. J.; Gao, Q.; Tan, H. H.; Jagadish, C.; Kim, Y.; Zhang, X.; Guo, Y. N.; Zou, J. Twin-free uniform epitaxial GaAs nanowires grown by a two-temperature process. *Nano Lett.* **2007**, *7* (4), 921–926.

(17) Bauer, J.; Gottschalch, V.; Paetzelt, H.; Wagner, G.; Fuhrmann, B.; Leipner, H. S. MOVPE growth and real structure of vertical-aligned GaAs nanowires. *J. Cryst. Growth* **2007**, *298*, 625–630.

(18) Wagner, R. S.; Ellis, W. C. Vapor-Liquid-Solid mechanism of single crystal growth. *Appl. Phys. Lett.* **1964**, *4* (5), 89.

(19) Cirlin, G. E.; Dubrovskii, V. G.; Sibirev, N. V.; Soshnikov, I. P.; Samsonenko, Y. B.; Tonkikh, A. A.; Ustinov, V. M. The diffusion mechanism in the formation of GaAs and AlGaAs nanowhiskers during the process of molecular-beam epitaxy. *Semiconductors* **2005**, *39* (5), 587–594.

(20) Dubrovskii, V. G.; Sibirev, N. V. General form of the dependences of nanowire growth rate on the nanowire radius. *J. Cryst. Growth* **2007**, *304* (2), 504–513.

(21) Givargizov, E. I. Fundamental aspects of VLS growth. *J. Cryst. Growth* **1975**, *31* (Dec), 20–30.

(22) Dubrovskii, V. G.; Sibirev, N. V. Growth rate of a crystal facet of arbitrary size and growth kinetics of vertical nanowires. *Phys. Rev. E* **2004**, *70* (3), 031604.

(23) Seifert, W.; Borgstrom, M.; Deppert, K.; Dick, K. A.; Johansson, J.; Larsson, M. W.; Martensson, T.; Skold, N.; Svensson, C. P. T.; Wacaser, B. A.; Wallenberg, L. R.; Samuelson, L. Growth of one-dimensional nanostructures in MOVPE. *J. Cryst. Growth* **2004**, *272* (1−4), 211–220.

(24) Johansson, J.; Svensson, C. P. T.; Martensson, T.; Samuelson, L.; Seifert, W. Mass transport model for semiconductor nanowire growth. *J. Phys. Chem. B* **2005**, *109* (28), 13567–13571.

(25) Dubrovskii, V. G.; Cirlin, G. E.; Soshnikov, I. P.; Tonkikh, A. A.; Sibirev, N. V.; Samsonenko, Y. B.; Ustinov, V. M. Diffusion-induced growth of GaAs nanowhiskers during molecular beam epitaxy: Theory and experiment. *Phys. Rev. B* **2005**, *71* (20), 205325.

(26) Plante, M. C.; LaPierre, R. R. Growth mechanisms of GaAs nanowires by gas source molecular beam epitaxy. *J. Cryst. Growth* **2006**, *286* (2), 394–399.

(27) Zhang, G.; Tatenoa, K.; Sogawa, T.; Nakano, H. Growth and characterization of GaP nanowires on Si substrate. *J. Appl. Phys.* **2008**, *103* (1), 014301.

(28) Dayeh, S. A.; Susac, D.; Chen, P.; Jing, Y.; Kavanagh, K. L.; Lau, S. S.; Yu, E. T.; Wang, D., Optimal control over the InAs nanowire growth for system integration and their structural and transport properties. *IEEE Nano* **2008**, in press.

(29) The NWs were imaged by a scanning electron microscope (SEM, Phillips XL30 ESEM) at a 20 kV acceleration voltage, with a 65° viewing angle. NW length data were extracted from the SEM images, corrected for the viewing angle, and averaged over samples of 15−40 wires growing in different locations of the substrate (i.e., at the center and near the edges). Such analysis yielded the average NW lengths (growth rates) and standard deviations (statistical errors) reported in the graphs.

(30) The temperature of the susceptor was calibrated by an optical pyrometer (Mikron M668) against a reference blackbody furnace (Instron SFL CL1192B, ±3 °C accuracy). The experimental error on the determination of the growth temperature was estimated to be ±5 °C, accounting for calibration errors and possible temperature drifts due to the different coating condition of the growth chamber. Gas flows were adjusted by analogue mass flow controllers, and the concentration of TMGa was measured directly by an in-line gas concentration monitor (Epison III).

(31) Paiano, P.; Prete, P.; Lovergine, N.; Mancini, A. M. Size and shape control of GaAs nanowires grown by metalorganic vapor phase epitaxy using tertiarybutylarsine. *J. Appl. Phys.* **2006**, *100* (9), 094305.

(32) Reep, D. H.; Ghandhi, S. K. Deposition of Gaas Epitaxial Layers by Organometallic Cvd - Temperature and Orientation Dependence. *J. Electrochem. Soc.* **1983**, *130* (3), 675–680.

(33) NP size dependence data are typically obtained by annealing a thin metal film to form discrete NPs by substrate dewetting. NWs grown from these NPs show a very broad size distribution. However, by this method, it is difficult to control the NP surface density (which is typically very high) and size frequency. The contact area between these NPs and the substrate is also different than the case of colloidal NPs and may vary as a function of size. Since all of these aspects are known to affect the NW morphology and growth rate, we preferred to conduct similar experiments by using a mixture of colloidal NPs with discrete size distributions and uniform NP density.
(34) Johansson, J.; Wacaser, B. A.; Dick, K. A.; Seifert, W. Growth related aspects of epitaxial nanowires. *Nanotechnology* **2006**, *17* (11), S355–S361.
(35) Chen, Z.; Cao, C. B. Effect of size in nanowires grown by the vapor-liquid-solid mechanism. *Appl. Phys. Lett.* **2006**, *88* (14), 143118.
(36) Following ref 24, P_∞ has been estimated as $P_\infty = x \cdot P_{vap}$, where P_{vap} is the Ga vapor pressure and $x = 0.1$ represents the fraction of Ga in the Au nanoparticle; $P_{vap} \approx P_0 \exp[(\Delta H_{vap}/R)(T_0^{-1} - T^{-1})]$, with $\Delta H_{vap} = 258.7$ kJ/mol and $P_0 = 9.31 \times 10^{-36}$ Pa at $T_0 = 302.9$ K. Alternatively, an empiric expression for P_{vap} is provided in *J. Electrochem. Soc.* **1962**, *109*, 144.: log P_{vap} (atm) $= -14900/T - 0.515 \log T + 7.34$. This expression provides values for P_{vap} approximately 1 order of magnitude lower than the previous method. Cochran, C. N.; Foster, L. M. Vapor Pressure of Gallium, Stability of Gallium Suboxide Vapor, and Equilibria of some Reactions Producing Gallium Suboxide Vapor. *J. Electrochem. Soc.* **1962**, *109*, 144.
(37) Stringfellow, G. B. A critical appraisal of growth mechanisms in MOVPE. *J. Cryst. Growth* **198468**, (1), 111–122.
(38) Larsen, C. A.; Li, S. H.; Buchan, N. I.; Stringfellow, G. B.; Brown, D. W. Kinetics of the reaction between trimethylgallium and arsine. *J. Cryst. Growth* **1990**, *102* (1−2), 126–136.
(39) Jensen, K. F.; Fotiadis, D. I.; Mountziaris, T. J. Detailed models of the MOVPE process. *J. Cryst. Growth* **1991**, *107* (1−4), 1–11.
(40) Wang, C. X.; Wang, B.; Yang, Y. H.; Yang, G. W. Thermodynamic and kinetic size limit of nanowire growth. *J. Phys. Chem. B* **2005**, *109* (20), 9966–9969.
(41) Stringfellow, G. B. Fundamental aspects of vapor growth and epitaxy. *J. Cryst. Growth* **1991**, *115* (1−4), 1–11.
(42) Hayakawa, T.; Morishima, M.; Chen, S. Surface reconstruction limited mechanism of molecular beam epitaxial growth of AlGaAs on (111)B face. *Appl. Phys. Lett.* **1991**, *59* (25), 3321–3323.
(43) Lim, S. K.; Tambe, M. J.; Brewster, M. M.; Gradecak, S. Controlled growth of ternary alloy nanowires using metalorganic chemical vapor deposition. *Nano Lett.* **2008**, *8* (5), 1386–1392.
(44) Verschuren, C. A.; Leys, M. R.; Vonk, H.; Wolter, J. H. Interfacet surface diffusion in selective area epitaxy of III-V semiconductors. *Appl. Phys. Lett.* **1999**, *74* (15), 2197–2199.

NL801986R